



Faculty of Women for, Arts,
Science, and Education



Scientific Publishing Unit



Journal of Scientific Research in Science

Basic Sciences

Volume 40, Issue 1, 2023

ISSN 2356-8372 (Online) \ ISSN 2356-8364 (print)





Contents lists available at EKB

Journal of Scientific Research in Science

Journal homepage: <https://jsrs.journals.ekb.eg/>



Graphene-based hydrogel silver nano-composites for antibacterial and antitumor applications: In vitro evaluation

Asmaa Kh. Atef^{1,*}, Tahia B. Mostafa¹, Hazem M. El-Sherif²

¹Chemistry Department, Faculty of Women for Art, Science and Education, Ain Shams University, Héliopolis, Cairo, Egypt.

²Polymers and Pigments Department, National Research Centre, Cairo, Egypt.

Abstract

The efficiency of most cancer therapies and antibiotics is restricted due to several issues, including medication resistance and non-specific negative effects. Hydrogels based on graphene derivative and silver nano-particles (Ag-NPs) have been employed to overcome these limitations. In this manuscript, we synthesized gelatin methacryloyl (Gel-MA) to combine with functional nano-materials. Reduced graphene oxide (rGO) was synthesized by utilising ascorbic acid as a green reductant to form a composite with Gel-MA without affecting its unique characteristics. The prepared rGO and nano-composite hydrogels were characterized by the usual characteristic spectroscopic techniques. We found that the nano-composite swelled up to 2444% due to the high porosity of the hydrogel. The results demonstrated that the nanocomposite hydrogel showed higher antimicrobial activities than virgin (Gel-MA). The cytotoxicity of Gel-MA/rGO and Gel-MA/rGO/Ag composites against human lung cancer (A549) cells was evaluated using MTT assay. The Gel-MA/rGO/Ag composite showed remarkable cytotoxicity with an IC₅₀ of 27μg/ml towards A549 cells compared with 109μg/ml of Gel-MA/rGO.

Keywords: Antibacterial, Antitumor, Gelatin, Gelatin methacryloyl, Hydrogel, Graphene nano-composites.

1. Introduction

Within the last few decades, there have been some growing warnings about cancer and microorganisms that have been threatening the world's healthcare system. Antibiotics are no longer as effective due to overuse and misuse, which have brought society to a continuous rise of antimicrobial resistance (AMR) [1]. On the other hand, cancer ranks as the second most common cause of death globally. The use of modern therapies, such as radiotherapy, chemotherapy, or a combination of them, has a significant negative influence on a patient's

*Corresponding author: Asmaa Kh. Atef, Chemistry Department, Faculty of Women for Arts, Science and Education, Ain Shams University, Egypt.

E-mail: asmaa.khaled@women.asu.edu.eg

(Received 01 December 2022, revised 02 December 2022, accepted 18 January 2023)

<https://doi.org/10.21608/JSRS.2023.178196.1097>

life. Moreover, recent studies demonstrate that, bacteria have adapted to traditional drug therapy and tumors are capable of developing a resistance toward chemotherapy treatments [2]. As a result, cancer and AMR are craving for an urgent solution far away from conventional treatments. Nanotechnology is introduced here as an adequate solution. The effect of nanotechnology into drugs comes from the effectiveness of the nano-structures' interactions with biological materials owing to their large surface area, making them highly reactive [3,4]. The technological advantages of nanoparticles used as drug carriers are high stability, high carrier capacity, feasibility of incorporation of both hydrophilic and hydrophobic substances, and feasibility of variable routes of administration, including oral application and inhalation [5]. **D. Kichukova et al.** [6] have reported that Ag-NPs nanocomposites are useful in fighting both cancer and bacterial infections.

Nowadays, biomaterials play a significant role in the diagnosis and treatment of many human diseases. Metals, ceramics, polymers, and composites are the four broad groups into which biomaterials can be categorized [7,8]. In recent years, there has been an increasing attention in the development of biomaterials resulting from renewable sources (e.g. silk, cellulose, collagen, and chitosan) since they are inexpensive and biocompatible [9,10]. They have been utilized to prepare different forms, such as films, scaffolds, and nanoparticles. Their main applications involve wound healing [11], drug carrier [12], pharmaceutical film coating [13], and muscle tissue engineering [14]. Fibrous proteins have a limited solubility in water or organic solvents, resulting from high intra-molecular hydrogen bonds and hydrophobic interactions, which is one of the major obstacles found in the processing of biomaterials [15].

Hydrogels are the best alternative to biomaterials to overcome their limitations. Since hydrogels are known as flexible three dimensional polymeric networks consisting of natural or synthetic polymers with remarkable properties such as hydrophilicity, biocompatibility, bio-functionality and elasticity, they are one of the ideal multipurpose materials in biomedicine [16]. The hydrophilic functional groups in the polymer structure are responsible for the high water absorption capacity. The amount of water absorption depends on the chemical composition of the synthetic polymer or biopolymer, the crosslinking density and the environmental conditions [17, 18]. Because of their typical moist and soft properties, which are highly comparable to biological tissue, hydrogels have been widely used in many biomedical applications [19].

Gelatin is one of the naturally occurring polymers that is a particularly bio-adhesive because it contains motifs for cell-binding like arginine-glycine-aspartic acid peptides. It is a

purified protein that is extracted from a connective tissue known as collagen [20]. Due to its good solubility and biocompatibility, gelatin is frequently used in the preparation of hydrogels. However, the poor mechanical performance of gelatin-based hydrogel is often improved by mixing/reacting with other polymers or nano-materials, such as derivatives of graphene and carbon nanomaterials. Consequently, there is a trade-off between biological and physical features when developing hydrogels [21].

Gelatin methacryloyl (Gel-MA) hydrogels have sustained the bioactivity and biocompatibility of the gelatin, thus they are the most researched soft materials for different medical purposes [22].

Graphene (Gr) has attracted a lot of interest due to its unique characteristics. As a biomaterial, Gr is frequently used in the preparation of composites because it can reduce inflammatory reactions in the human body and improving the biocompatibility. Furthermore, the large specific surface area of Gr facilitates the binding, absorption, and delivery of targeted molecules [23].

Graphene oxide (GO) has a smaller surface area compared to graphene. It is exfoliated from graphite flakes, involving of few layers. The edges of the GO layers are mostly occupied by carboxyl and carbonyl groups in a random pattern, while the basal planes are decorated with hydroxyl and epoxide functional groups [24]. There are many methods for the reduction of GO, such as the thermal, optical, and chemical ones. Among these methods, the chemical one is the most popular and depends on many types of reducing agents [25]. We performed an oxidation process using the hummers' method to produce GO, followed by a green reduction method using ascorbic acid (vitamin C) to obtain reduced graphene oxide (rGO) [26].

Ur Rehman et al. [27] developed a hydrogel fabricated with graphene derivatives as an effective dressing material to enhance cell migration, proliferation, and antibacterial property. The sharp edges of rGO resulted in physical damage to the bacteria's cell-wall and membrane [28]. Besides, it was concluded that the oxidative stress caused by rGO nano-sheets or/and Ag-NPs creates an imbalance in the generation of reactive oxygen species followed by bacterial cell death [29]. Oxygen-containing groups can enhance the dispersion property of rGO in organic or aqueous system. Therefore, it is desirable to use rGO in the manufacture of composite materials. The biomedical applications of rGO are still the topic of several research studies to date [30].

P. Jose et al. found that the major limitation of the antibacterial properties of Ag-NPs is their agglomeration, so loading of Ag-NPs on proper supporting matrices may be necessary to prevent such agglomeration and increase antibacterial efficiency [31]. Several valuable elements, especially silver or gold, present anticancer and antimicrobial activity with a minimal related cytotoxicity [32].

This work was engaging with the synthesis and evaluation of Gel-MA/rGO and Gel-MA/rGO/Ag composites against some model bacteria and human lung cancer cells in order to study the synergistic effect of both particles and to improve their antimicrobial and anticancer effect. We also performed cytotoxicity against human lung cancer (A549) cells in vitro to verify the possibility of using these composites as a clinically active chemotherapy agent. The Gel-MA/rGO/Ag composite presented a significant anticancer ability with an IC₅₀ value of 27µg/ml. The prepared nano-composites gave promising results in both fields of applications.

2. Materials and methods

2.1. Materials

Gelatin from bovine skin (type B with gel strength of ~225 g Bloom), Methacrylic anhydride (MAA 94%, contains 2,000 ppm topanol A as an inhibitor) and 2-hydroxy-4'-(2-hydroxyethoxy)-2-methylpropiophenone (Irgacure 2959) as a photo-initiator were received from Sigma-Aldrich, USA. Hydrochloric acid (HCl, 38%), sodium hydroxide (NaOH), sodium carbonate (Na₂CO₃), sodium bicarbonate (NaHCO₃) and 98% pure graphite fine powder were obtained from LOBA CHEMIE PVT. LTD., India. Sulphuric acid (H₂SO₄, 98%), hydrogen peroxide (H₂O₂, 30%), potassium permanganate (KMnO₄), potassium nitrate (KNO₃), phosphoric acid (H₃PO₄), were obtained from BDH Chemicals Ltd., England. Ascorbic acid (vitamin C, C₆H₈O₆), ethanol (C₂H₅OH, 99%), potassium chloride (KCl), sodium chloride (NaCl), di-sodium phosphate (Na₂HPO₄), mono-potassium phosphate (KH₂PO₄) and ninhydrin (2,2-Dihydroxy-1H-indene-1,3-(2H)-dione, C₉H₆O₄) were bought from "El-Gomhouria Co. For Drugs & Chemicals", Egypt. Distilled water (DW) was used through this study. All chemicals were used without any further purification.

2.2. Methodology

2.2.1. Synthesis of Gelatin-methacryloyl (Gel-MA) from Methacrylic anhydride

In brief, a 10% (w/v) gelatin (type B) solution was dissolved under stirring in 0.25M carbonate/bicarbonate buffer (CB, pH 9.4) at 50°C. The modification process was initiated by the successive addition of MAA under rigorous stirring at 500 rpm at the same temperature,

according to the desired ratio [x ml MAA/g gelatin, namely, 0.1:1 designated as (M1), and 1:1 as (M2)]. After each addition, the pH was brought back to 9.4 using 5N NaOH. The reaction was performed for 180 min and completed by pH adjustment to 7.4, using 1N HCl. Then, the mixture was purified using the conventional Whatman™ grade 1 filter paper (GE Healthcare Life, Little Chalfont, Buckinghamshire, UK) and dialyzed against ultra-pure water for 36 h at 40°C using a molecular weight cut-off (MWCO) membrane of 14kDa (Carl Roth GmbH & Co. KG, Karlsruhe, Germany). To ensure complete elimination of low molecular weight gelatin and methacrylic acid reaction by-products, water was changed every 4 h. After dialysis, the Gel-MA solution was frozen and then followed by lyophilization. The obtained dry pale-yellow Gel-MA product was kept in dark at 4°C.

2.2.2. Preparation of Gel-MA Hydrogels

Gel-MA hydrogels were produced by dissolving the 10%, w/v of the desired Gel-MA solution in 0.01M phosphate-buffered solution (pH 7.4) at 50°C. Then 0.5% w/v Irgacure 2959 was added to launch the photoreaction using UV light at 365 nm (CL-1000, UV cross-linker, Funakoshi Co., Ltd., Tokyo, Japan) for 15 min at a distance of 10 cm. After curing, the prepared hydrogels were cut into discs with 10 mm & 2 mm diameter and thickness, respectively.

2.2.3. Graphene oxide (GO) Synthesis from graphite powder

GO was developed using a modified Hummer's approach [33]. Briefly, 1 g graphite and 9.89 mmol KNO₃ were mixed with 50 ml conc. H₂SO₄ & 3 ml H₃PO₄ and stirred for 120 min in an ice bath. Afterward, 37.96 mmol KMnO₄ was added gradually at a slow rate to keep the mixture's temperature below 5°C. Then, the suspension was stirred in an ice bath for 2 h and then at 40°C for 60 min. The suspension color progressively changed from black to deep green once KMnO₄ was slowly added. Then, the suspension was transferred into a water bath with a temperature of (40-50°C) under continuous stirring for about 24 hours until the color of the suspension became pasty brownish. The mixture was then brought to a steady temperature of 98°C for 30 min while water was added slowly under continuous stirring. Therefore, distilled water (DW) was added in order to make the volume of the suspension 400 ml and the color changed to dark brown suspension. Last of all, 3 ml of H₂O₂ (30%) was added slowly drop by drop to the solution with effervescence to neutralize excess of potassium permanganate.

By using BaCl₂ solution, the elimination of the metal sulphate ions was confirmed. The supernatant was decanted away after 4 h of centrifugation at 4000 rpm for washing operation.

The pH of the obtained material (GO) was adjusted using a pH indicator to be around 7 and stirred in DW water at room temperature for 24 h.

2.2.4. Reduced graphene oxide (rGO) synthesis

In order to chemically reduce GO to rGO, ascorbic acid (5.67 mmol) was dissolved into a previously sonicated homogeneous brown dispersion of 100 mg of GO per 10 ml of DW in a water-cooled condenser system. Then the temperature was elevated to 95°C for approximately 30 h. The as-prepared rGO was vacuum-filtered and dried at room temperature overnight [34].

2.2.5. Preparation of Gel-MA/rGO composite

In order to prepare rGO hydrogel composite, 0.2% rGO was added to the 10% Gel-MA (M1) pre-polymer solution in PBS, sonication was done for an hour to obtain a homogeneous mixture. The aforementioned procedure, illustrated in section 2.2.2., was followed to form Gel-MA/rGO hydrogel.

2.2.6. Preparation of Ag nano-composite

About 50 mg of lyophilized hydrogel discs (Gel-MA/rGO) were immersed in DW for 2 days. The swelled discs were placed in a beaker with 50 ml of 0.01M aq. AgNO₃ and then kept for one day to equilibrate at room temperature to anchor silver ions to the -NH₂, -OH groups of polymeric chains or drive silver ions into the gel networks free-spaces. Then, the silver-loaded hydrogels were blotted with a tissue paper and transferred to a beaker with 50 ml of cold 0.1M aq. NaBH₄ solution. For three hours, the beaker was placed in a 4°C refrigerator to convert the silver ions into silver nanoparticles.

2.3. Physico-Chemical Characterization

2.3.1. FT-IR Spectroscopy

To confirm the formation of the hydrogels and graphene materials, FT-IR analysis was utilized by Nicolet IS 10, Thermo Fisher Scientific spectrophotometer (at the Central Lab, Ain Shams University, Egypt), employing KBr pellets with wavenumbers between 4000 and 400 cm⁻¹.

2.3.2. UV- visible Spectroscopy

UV measurements for the suspension of GO, rGO and Ag nano-particles were carried out by using Thermo Scientific Evolution 300 UV-Vis spectrophotometer (at the Central Lab,

Ain Shams University, Egypt), which has a xenon flash lamp light source with a spectral range of 190–600 nm, and a double beam optical design.

2.3.3. X-Ray Diffraction analysis (XRD)

The X-ray diffraction (XRD) pattern of GO, rGO and the prepared hydrogels was recorded on a powder X-ray diffractometer, Rigaku MiniFlex, Central Metallurgical Research Institute, Egypt.

2.3.4. Raman Spectroscopy

Raman spectroscopy is an effective method for identifying carbonaceous materials and in particular for detecting disorder in the crystal lattices of carbon. GO reduction was identified by Raman spectrometer (Wi Tec 300 R, Raman scope, Germany, 532 nm laser line, National Research Center, Egypt).

2.3.5. Scanning Electron Microscope analysis (SEM)

Morphological analysis of Gel-MA and Gel-MA/rGO lyophilized hydrogels was performed by scanning electron microscopy (SEM). The hydrogel discs were frozen and lyophilized. Then, the lyophilized hydrogel discs introduced into SEM (Zeiss EVO 15, National Centre for Radiation Research, Egypt) chamber for imaging. The samples were placed on a metal stub with double adhesive tape and coated with gold under vacuum.

2.3.6. Transmission Electron Microscope (TEM)

The samples were prepared for TEM analysis by sonication for 30 min then a drop of the suspension was applied on the carbon coated with copper grids and dried by permitting water to evaporate at room temperature. Electron micrographs were produced using JEOL GEM-1010 TEM at 80 kV (at the Regional center for Mycology and Biotechnology, Al- Azhar University, Egypt).

2.3.7. Energy Dispersive X-ray Spectroscopy (EDX)

EDX analysis is a widely used analytical technique for determining the chemical composition of materials with an energy dispersive X-ray spectroscopy (EDX system attached with FESEM) using a Zeiss EVO 15, at the National Center for Radiation Research, Egypt.

2.3.8. Vacuum freeze dryer

The BIOBASE, Model Country freeze-dryer (National Research Center, Egypt) was used for lyophilization. The drying conditions were -43°C & a vacuum of 00031 Pa.

2.4. Determination of degree of functionalization (DF %) (Ninhydrin assay)

Both the lyophilized gelatin and Gel-MA specimens were dissolved in 0.01M PBS. To construct a successful standard curve, PBS was used to serially dilute untreated gelatin from 0 to 6 mg/ml. Also, the modified gelatin specimens were in triplicate without any dilution. A 0.22 % w/vol. ninhydrin ethanolic solution was applied to each specimen in a 1:8 v/v ratio of ninhydrin to gelatin or modified gelatin solutions. The tubes were kept in a 90°C oven until a regular pattern of color development was noticed (after about 30 min). The absorbance values were determined at 570 nm and then the average absorbance for each gelatin concentration was plotted to form the standard curve [35]. For each modified sample, the fraction of the available amine groups that were present was calculated using equation (1).

$$\text{Fraction of the available amine groups} = \left(1 - \frac{\text{Apparent specimen conc.}}{\text{Nominal specimen conc.}} \right) \quad (1)$$

As the apparent specimen concentration was determined via the standard curve and the nominal specimen concentration was calculated, the DF (%) was determined by equation (2).

$$\text{DF (\%)} = 100 \times \left(1 - \frac{\text{Apparent specimen conc.}}{\text{Nominal specimen conc.}} \right) \quad (2)$$

2.5. Equilibrium swelling study

When a hydrogel disc is submerged in water, it expands until the elastic forces from the stretched segments of the polymer balance the osmotic forces that serve to extend the polymer network. The swelling behavior of hydrogels was evaluated by dipping the lyophilized hydrogel discs in PBS at (pH = 3, 7.4, and 8) and DW at 37°C to simulate physiological media. The swelling behavior was evaluated by measuring the absorption of PBS into the hydrogels gravimetrically at specific time periods till equilibrium. The samples were carefully wiped off with filter paper before weight measurements to remove any superficial water. The percentage of swelling was measured using Equation (3).

$$\text{Swelling Percentage (\%)} = \left(\frac{W_{\text{rehydrated}} - W_{\text{freeze-dried}}}{W_{\text{freeze-dried}}} \right) \times 100 \quad (3)$$

Where $W_{\text{rehydrated}}$ refers to the weight of hydrogel after rehydration in PBS and $W_{\text{freeze-dried}}$ refers to the weight of hydrogel after lyophilization.

2.6. Porosity of hydrogels

Hexane displacement method was employed to determine the porosity of the prepared hydrogels. In brief, hydrogels were cut into smaller discs of equal dimensions. A screw gauge was used to measure their height and diameter, and subsequently their volumes were calculated. Hydrogels were then submerged in an n-hexane solution for 30 min to allow hexane to fill the pores inside the hydrogel network. The hydrogels were eventually taken out of hexane and weighted [36]. The porosity of hydrogels was estimated using the equation (4).

$$\text{Porosity of hydrogels (\%)} = \left(\frac{W_2 - W_1}{\rho \times V} \right) \times 100 \quad (4)$$

Where ρ is the density of n-hexane (0.665-0.683 g/ml), V is the volume of the hydrogel discs, and W_1 , W_2 are the weights of the hydrogel before and after 30 minutes of immersion in n-hexane, respectively. These experiments were carried out in triplicates and the average values were calculated.

2.7. Antimicrobial assay (Disc diffusion method)

The antibacterial activity of the hydrogel discs was investigated with respect to four bacteria strains. All hydrogels were tested in vitro against *Staphylococcus aureus* (*S. aureus*, ATCC25923) and *Bacillus subtilis* (*B. subtilis*, RCMB 015 (1) NRRL B-543) as gram positive (+ve) bacteria and versus *Escherichia coli* (*E. coli*, ATCC 25922) and *Proteus vulgaris* (*P. vulgaris*, RCMB 004 (1) ATCC 13315) as gram negative (-ve) bacteria using disc diffusion method. Turbid bacterial suspensions were swabbed evenly onto agar plates. After drying the surfaces of the plates, they were kept at 37°C for 24 hours under anaerobic environments after being dried. Antibiotic (e.g. Gentamycin) was spread on an agar plate pre-inoculated via filter paper discs impregnated with a specified antibiotic concentration (4µg/ml). Quantitative evaluation of susceptibility was performed by determining the diameter of the growth inhibition zone, including the diameter of the disk (in millimeters).

2.8. Cell culture (In vitro cytotoxicity studies)

Mammalian cell lines: Human Lung Carcinoma (A549) was received from the American Type Culture Collection, ATCC, Rockville, MD.

2.8.1. Evaluation of cytotoxicity assay

The A549 cells were diffused in 96-well tissue culture plate (at concentration of 5×10^4 cells/well) and then incubated for 1 day. The tested composites were then placed into 96-

well plate (three replicates) for each composite. For each 96-well plate, six vehicle controls (with media or 0.5% DMSO) were run as a control. After incubation, the standard methylthiazole-tetrazolium (MTT) assay was used for measuring cell viability. In brief, the media were withdrawn from the 96 well plates and replaced with 100 μ l of fresh culture medium (RPMI 1640) without phenol red. Then 10 μ l of MTT stock solution (5 mg in 1 ml of PBS of MTT) was supplied to each well, the untreated controls are also included, and subsequently incubated at 37°C for 4 h. An aliquot (85 μ l) of the media was withdrawn from the wells, and 50 μ l of DMSO was replaced to each well then used the pipette to thoroughly mix it well and incubated for 10 min at 37°C. The optical density (OD) was determined at 590 nm with the microplate reader, SunRise, TECAN, Inc, USA [37].

Cell viability (%) = OD of tested sample/OD of untreated control.

2.8.2. Microscopic Observation of A549 cells

This experiment was carried out as previously stated in the antitumor activity protocol. After the treatment at the tested concentration was finished, the wells were turned over to remove the medium. They were then cleaned with PBS (pH 7.2), and the cells were fixed to the well for 15 min at room temperature using formalin solution (10%).

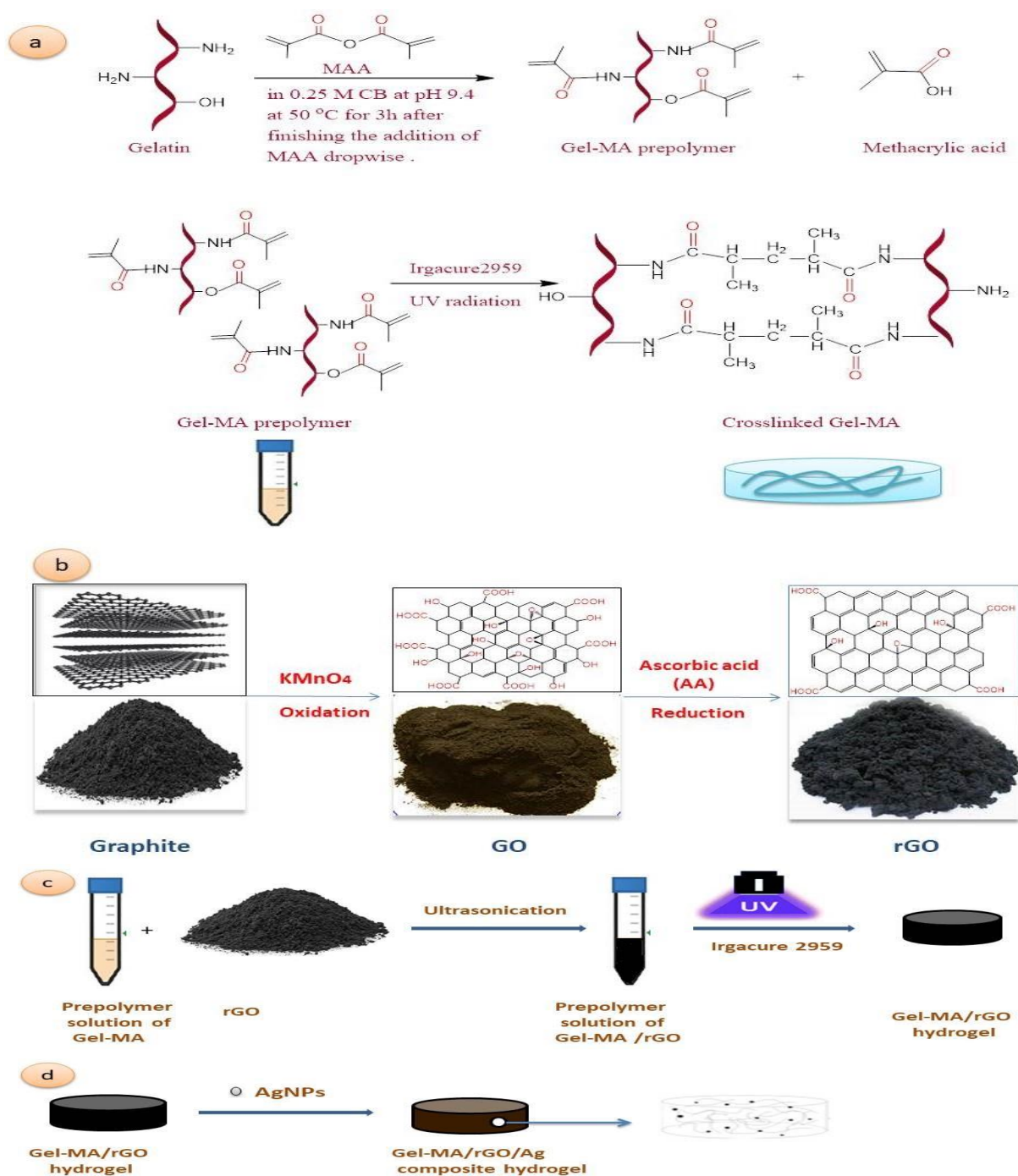
Then, 0.25% crystal violet (100 μ l) was used to dye the fixed cells for 20 min. After the stain was eliminated, the wells were rinsed with DI water to get rid of any remaining stain, and then they were let to dry. The morphology variations of the cells were examined using an inverted microscope (CKX41; Olympus, Japan) at 100x magnifications.

3. Results and discussion section

3.1. Synthesis of Gel-MA, Gel-MA/rGO and Gel-MA/rGO/Ag hydrogel composites

Gel-MA hydrogel as shown in **Fig. 1a** was synthesized according to previously reported method, in which methacryloyl functional groups were introduced to the gelatin backbone through condensation process between MAA with amine and hydroxyl groups of gelatin according to **Scheme 1a**. In this work, we used MAA as it is a photo-curable monomer. Thus the hydrogel synthesis was via UV light. Irgacure 2959 was selected as the photoinitiator due to its low toxicity and its biocompatibility. Also, we utilized ascorbic acid, an organic substance that occurs naturally, to reduce GO to rGO at 95°C. A successful reduction of GO was indicated by a change in the color of the solution. The GO solution was initially brownish in color, but after the reduction procedure, it became black as shown in **scheme 1b**.

Scheme 1c illustrates sonication of rGO within the prepared hydrogel substrate, to prevent the aggregation of the amphiphilic rGO layers and followed by the curing process as shown in **Fig. 1b**. A Gel-MA hydrogel was developed to serve as a model for immobilizing silver nanoparticles. When the swollen hydrogel was added to the silver nitrate solution, the ion exchange mechanism led to the anchoring of Ag^+ ions with the functional groups followed by the reduction of Ag^+ by NaBH_4 as shown in [scheme 1d].



Scheme 1. Synthesis of (a) Gel-MA hydrogel from MAA, (b) reduced graphene oxide (rGO), (c) Gel-MA/rGO hydrogel and (d) Gel-MA/rGO/Ag composite.

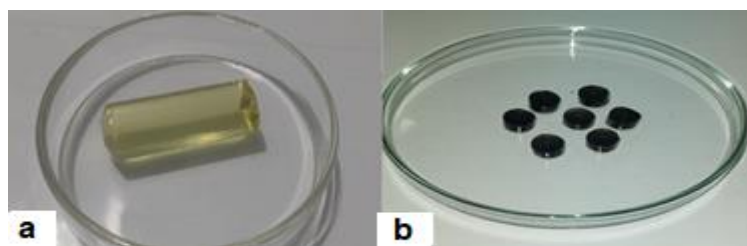


Fig. 1. Hydrogels (a) Gel-MA (M1) in cylindrical form and (b) Irradiated Gel-MA/rGO composite hydrogel discs.

3.2. Characterization of graphene materials and Gel-MA nano-composite hydrogels

3.2.1. FT-IR Spectroscopy

Fig. 2a-g represents the FT-IR of graphite, GO, rGO, gelatin, Gel-MA(M1) designed as a low functional hydrogel, Gel-MA(M2) designed as a high functional hydrogel, and Gel-MA/rGO composite. The spectra of gelatin, (M1) and (M2) (**Fig. 2d-f**) exhibit the characteristic peaks at 1331 cm^{-1} and 1555 cm^{-1} , due to the vibration mode of C–N–H bonds (amide I and II, respectively), at 1644 cm^{-1} corresponds to the C=O bonds, at 2979 cm^{-1} related to the C–H peaks and also at 3418 cm^{-1} refers to N–H bonds [38]. The strong peak of C=O stretching vibration appeared at 1644 cm^{-1} . This is because C=O on the amide has been shifted from the acid anhydride. These results confirmed that the Gel-MA has been synthesized successfully as illustrated in **Fig. 2e,f** taking into consideration the degree of functionalization according to the percentage of MAA [39]. Furthermore, The FTIR spectrum of GO shows distinct peaks at 3419 cm^{-1} (O–H stretching), $2923, 2854\text{ cm}^{-1}$ (asymmetric and symmetric CH_2 stretching), 1731 cm^{-1} (C=O stretching), 1627 cm^{-1} (C=C stretching), 1384 cm^{-1} (O–H bending), 1276 cm^{-1} (C–OH stretching), and 1075 cm^{-1} (C–O–C stretching) compared to the graphite shown in **Fig. 2a,b**. After reduction of GO, the peaks in the spectral region from 1500 to 1000 cm^{-1} became smaller due to the elimination of some oxygen-containing groups and the peak at 1731 cm^{-1} that relates to C=O stretching was diminished [40]. The corresponding peaks in rGO had smaller intensities as compared to that of GO as shown in **Fig. 2b,c**. Successful composite synthesis of Gel-MA/rGO was established by comparing the FTIR spectrum of Gel-MA/rGO to that of Gel-MA(M1) as illustrated in **Fig. 2g**. The spectrum consists of the characteristic absorption bands of both Gel-MA(M1) and rGO; taking into consideration that the intensity of the broad band at 3443 cm^{-1} (stretching of –OH groups) was significantly higher in the Gel-MA/rGO compared with that of Gel-MA(M1) and rGO [41].

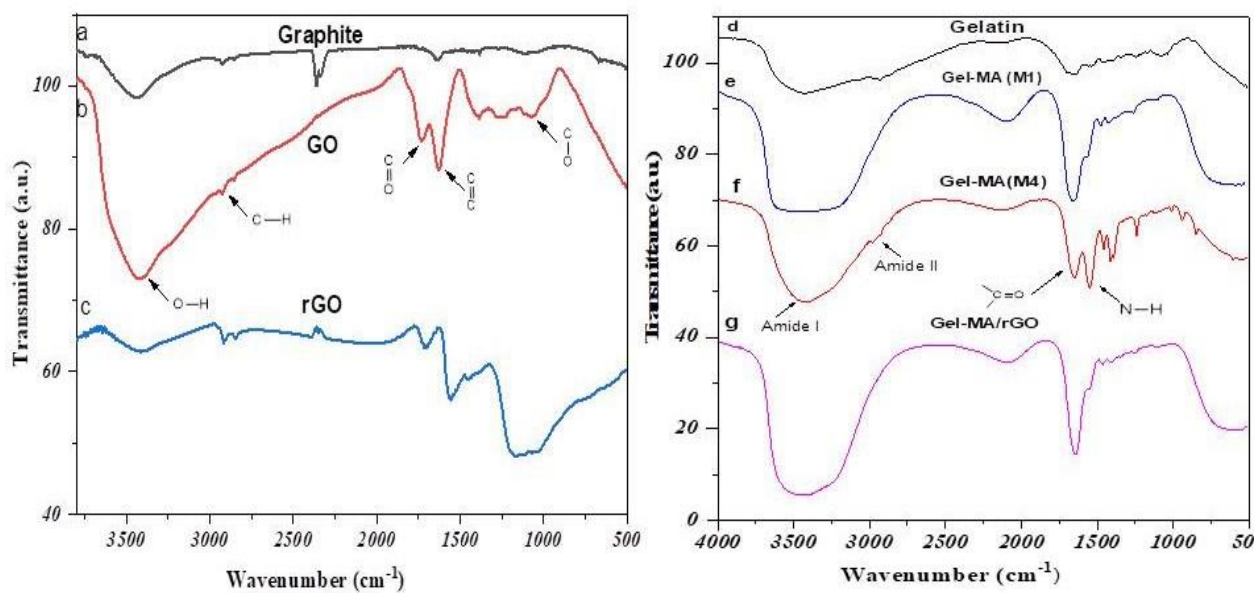


Fig. 2. FT-IR spectra of a) Graphite, b) GO, c) rGO, d) Gelatin, e) Gel-MA(M1), (f) Gel-MA(M2) and g) Gel-MA/rGO composite.

3.2.2. UV-visible spectroscopy

Fig. 3a shows the spectrum of pristine GO, a significant absorption peak can be observed at 232 nm, which was attributed to $\pi-\pi^*$ transitions of the C–C aromatic bond. After the reduction method, the absorption peak of GO was red-shifted to 270 nm due to the successful completion of deoxygenation process as shown in **Fig. 3b**. The absorption peak at 270 nm arises from the $n\rightarrow\pi^*$ electron transitions as well as the restoration of the electronic conjugation within graphene [42]. Thus, this technique can prove the successful reduction of GO into rGO via green chemistry.

While **Fig. 3c** illustrates a band appearance at 413 nm which may be attributed to the surface resonance of Ag-NPs. This result indicates the presence of Ag-NPs on rGO layers. The color of composite hydrogel turns from black to deep brown and the absorption peak at 413 nm confirms that silver ions (Ag^+) was reduced to silver nanoparticles [43].

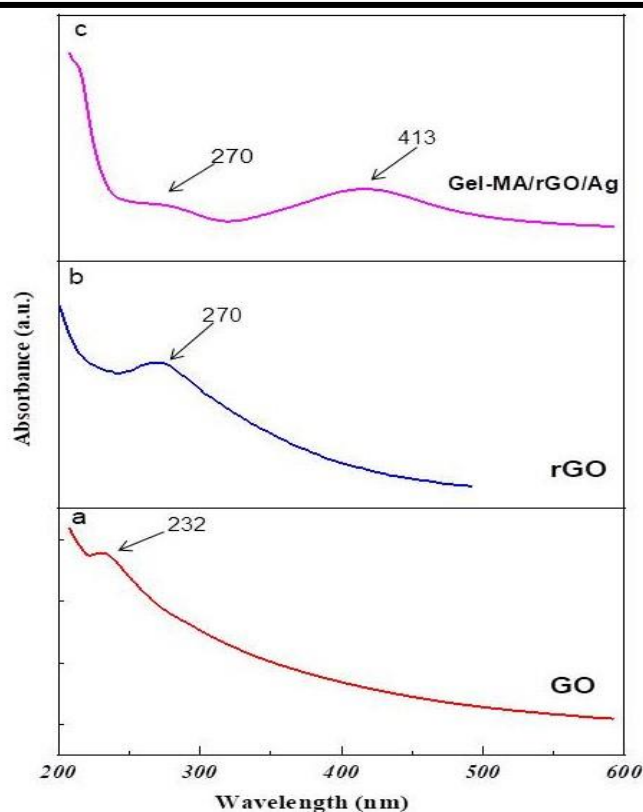


Fig. 3. UV–vis spectra of a) GO, b) rGO and c) Gel-MA/rGO/Ag composite.

3.2.3. X-ray Diffraction analysis (XRD)

Fig. 4a displays the X-ray diffraction pattern of graphite, GO and rGO. The X-ray diffraction showed a characteristic peak of graphite powder at $2\theta=26.4^\circ$. This peak was shifted towards a characteristic (001) broad reflection peak at $2\theta=9.6^\circ$, with inter-layer spacing distance of 9.16\AA between the GO layers. This proves the effective exfoliation and oxidation for GO sheet from graphite powder, since the d-spacing value was significantly higher than that of the natural graphite (3.48\AA). The reduction of GO to rGO resulted in a broad distinctive (002) reflection peak at $2\theta=23.7^\circ$, indicating a successfully restored conjugate structure [44]. While the XRD patterns of Gel-MA and Gel-MA/rGO/Ag nanocomposite are shown in **Fig. 4b**.

The pure Gel-MA hydrogel only had one broad peak centered around at $2\theta=24^\circ$ links to the polymer structure [45]. The phase change of the sample in the process of fabrication of Gel-MA/rGO/Ag nanocomposite was characterized using XRD. The XRD pattern of Gel-MA/rGO/Ag nanocomposite showed that the rGO peak overlapped by the main peak of Gel-MA around at $2\theta=24^\circ$ and the other peak at about $2\theta=38^\circ$ corresponding to Ag nanoparticles. The peak at $2\theta=38^\circ$ associated with the crystal planes (111) of Ag-NPs [46].

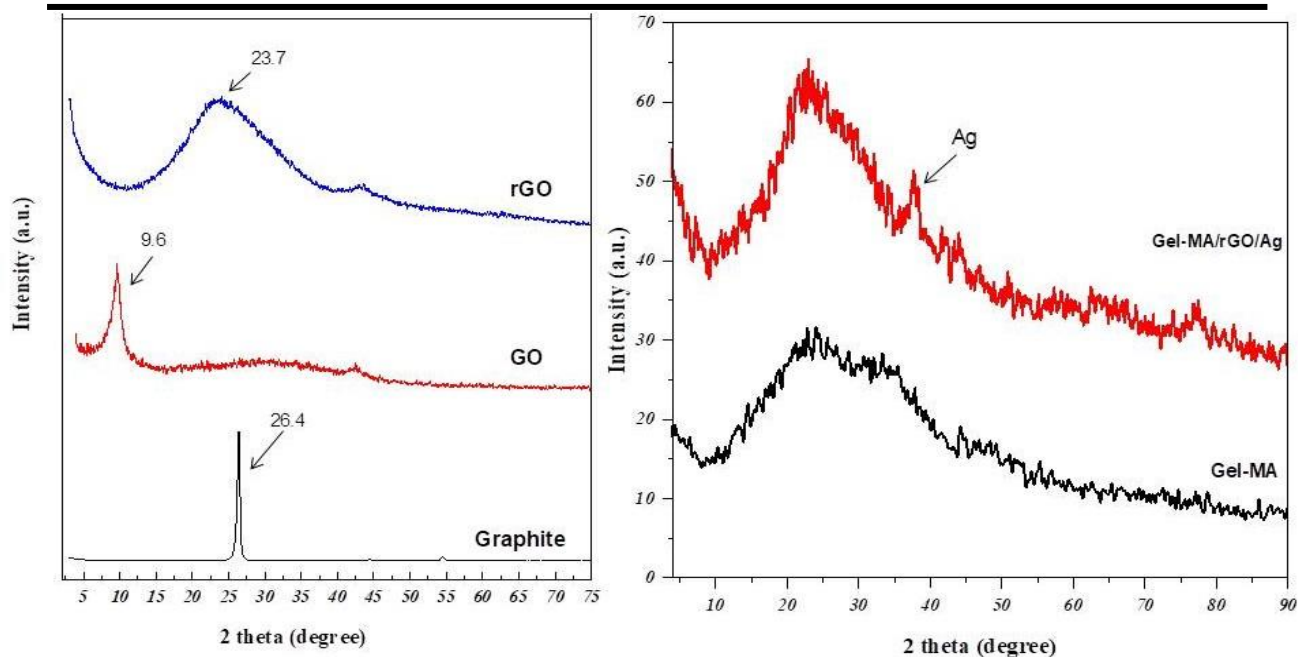


Fig. 4. XRD spectra of a) Graphite, GO and rGO b) Gel-MA hydrogel and Gel-MA/rGO/Ag composite.

3.2.4. Raman Spectroscopy

Raman spectroscopy is a widely used characterization process to evaluate the nature of defects and disorders of carbon materials. **Fig. 5** shows two distinctive peaks for GO, the major two significant peaks at 1354 cm^{-1} and 1602 cm^{-1} , which represent the diamondoid (D) and the graphitic (G) bands of GO, respectively. The G band is a result of simultaneous in-plane vibrations of symmetry sp^2 bonded carbon atoms whereas the D band is owing to the out of plane vibrations of disordered carbon atoms due to the structural defects in the lattice. The chemically modified graphite materials have large intensity of the D band may be due to the structural defects present on the edges of GO. The increase in D band intensity can be attributed to the conversion of sp^2 carbon to sp^3 one [47]. For rGO, the D band became broader owing to the higher disorder level of the graphene layers. Thus, the ratio between the D and G band intensities (I_D/I_G ratio) often indicates the disorder degree in a carbon framework confirming the reduction process of GO. The I_D/I_G ratios of GO and rGO were 0.77 and 0.98, respectively. The high I_D/I_G value of rGO indicates the high defect content in the structure which confirms the reduction process.

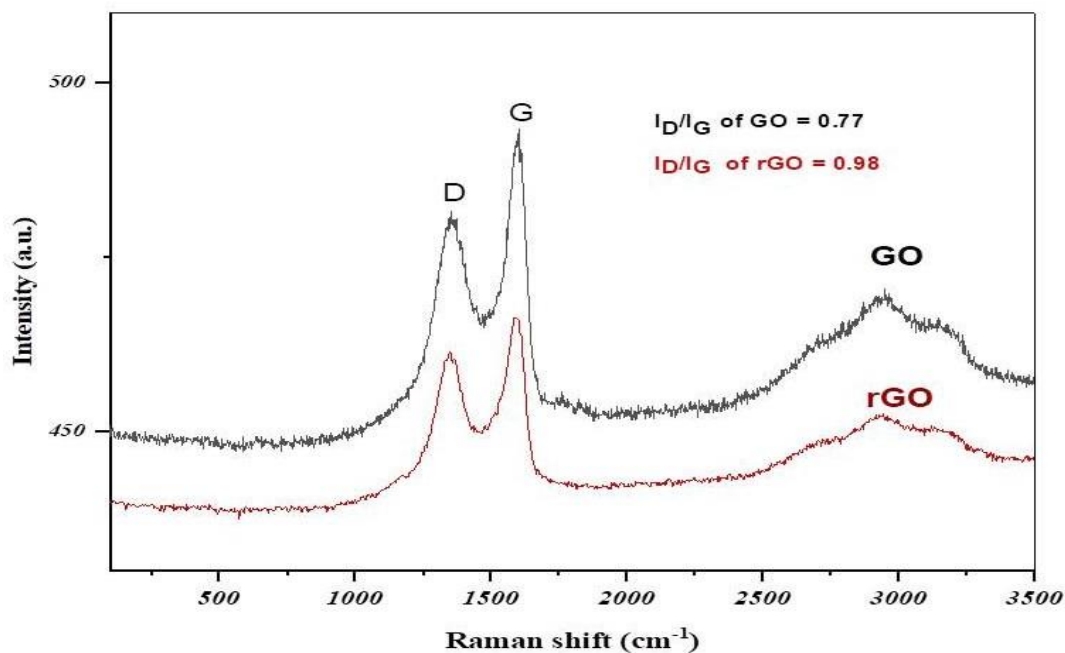


Fig. 5. Raman spectra of GO, and rGO.

3.2.5. Scanning Electron Microscopy (SEM)

In this study, the microstructures of Gel-MA(M1) and Gel-MA/rGO lyophilized hydrogels were observed by SEM, as shown in Fig. 6a,b, respectively. The results reveal that both Gel-MA(M1) and Gel-MA/rGO hydrogels possess a large pore surface morphology. Both display circular shaped micro-porous morphology. The pore size of Gel-MA(M1) was 80 μ m which makes these hydrogels good candidates for scaffold application as the high porosity of the hydrogel facilitates cellular migration and proliferation. The rGO was present in small percentages so the internal structure and the pore size of the nano-composite hydrogel were not considerably affected.

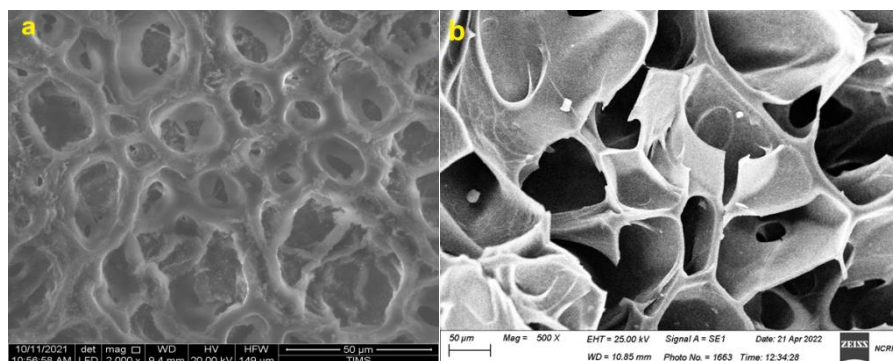


Fig. 6. SEM micrographs of a) Gel-MA(M1) hydrogel and b) Gel-MA/rGO composite hydrogel.

3.2.6. Transmission Electron Microscopy (TEM)

The morphological features of rGO and Gel-MA/rGO/Ag nanocomposite were confirmed by TEM analysis and carried out at 80 kV. In **Fig. 7a**, rGO displays a spherical pattern architecture with a size of 8-10 nm with some agglomeration using Magnification at 80000 \times . While **Fig. 7b** shows that the silver is nano-sized and dispersed and most of the Ag-NPs have an average diameter of 15 nm. The adhered Ag-NPs have spherical morphologies.

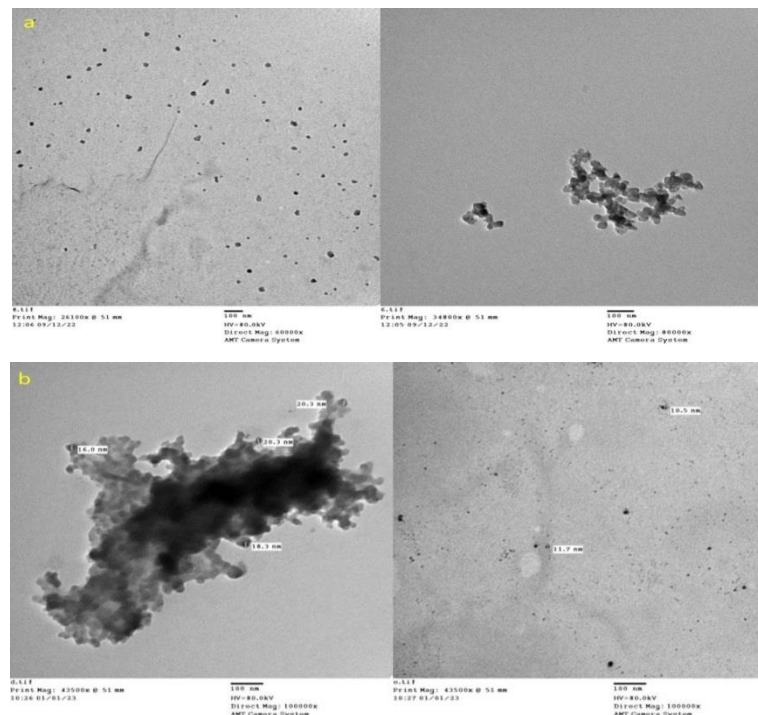


Fig. 7. TEM images of a) rGO and b) Gel-MA/rGO/Ag composite.

3.2.7. Energy Dispersive Spectroscopy (EDX)

EDX gives an idea about the elemental analysis of the biosynthesized nanoparticles. The EDX profile of Gel-MA/rGO/Ag composite [as shown in **Fig. 8**] demonstrates a strong signal for the Ag atoms present, and thus it indicates the presence of Ag phase in the composite. The C and O signal basically derives from rGO layers.

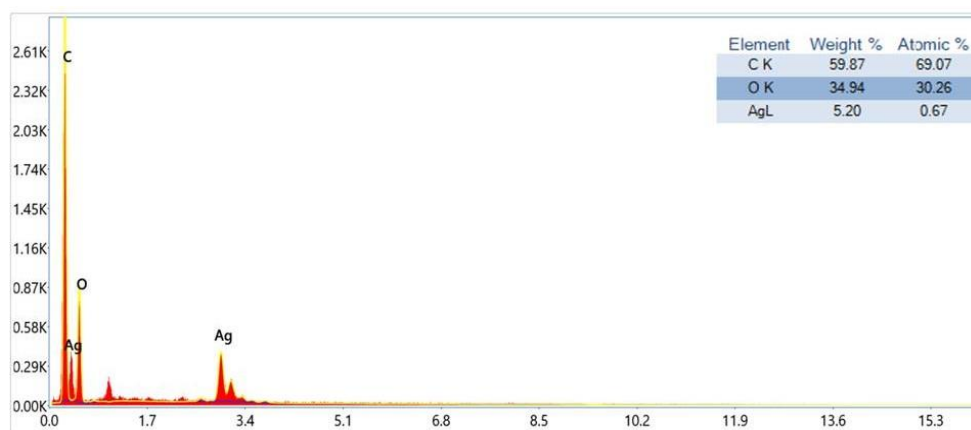


Fig. 8. EDX of Gel-MA/rGO/Ag composite.

3.2.8. Degree of functionalization (ninhydrin assay)

When the methacrylate functional groups in MAA attached to the free amine ($-\text{NH}_2$) groups in gelatin, we assessed the extent of functionalization by identifying the free amine groups in gelatin and Gel-MA samples as shown in **Fig. 9a,b**, respectively. The ninhydrin assay produces a colored ninhydrin chromophore called Ruhemann's purple when reacting with $-\text{NH}_2$ groups in the unmodified gelatin and in Gel-MA [48]. Two sets of Gel-MA were generated with low [Gel-MA(M1)], and high [Gel-MA(M2)] degree of functionalization (%) according to the percentage of MAA. The results revealed the ability to generate Gel-MA with a degree of functionalization varying approximately from 49% to 96%, respectively.

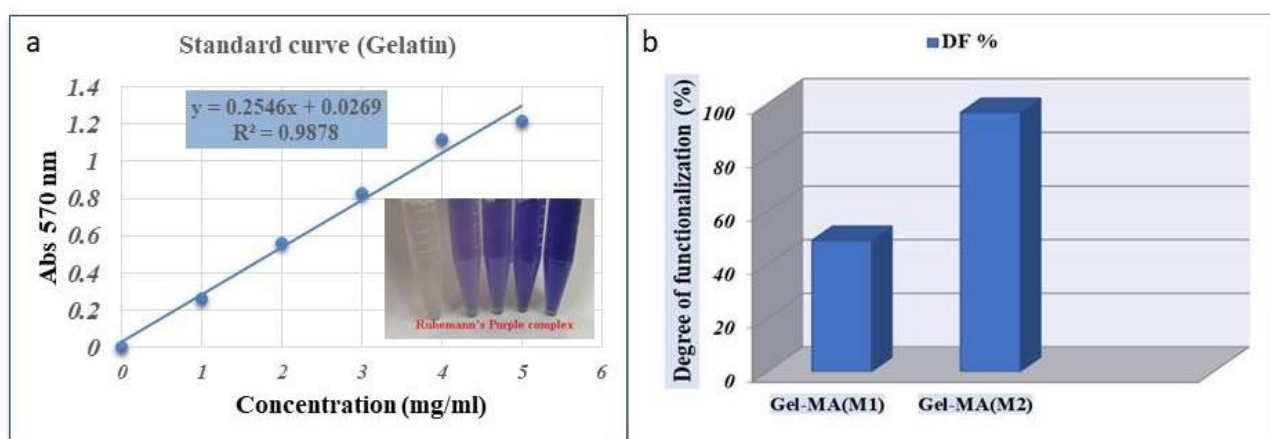


Fig. 9. (a) Standard curve of gelatin by using ninhydrin assay the inset represents Ruhemann's purple complex, and (b) degree of functionalization of Gel-MA according to the percentage of MAA

3.2.9. Swelling behavior

The swollen hydrogels gelatin, Gel-MA(M1), Gel-MA(M2) and Gel-MA/rGO were characterized by studying the swelling behavior in simulating buffer solutions at different pH (3, 7.4, 8) and in DW. The swelling ability of the Gel-MA at low and high degree of functionalization and nano-composite hydrogels were studied to evaluate the absorption capacity of the hydrogels. The swelling rate of both Gel-MA and nano-composite hydrogels increased significantly during the first 10 min of immersion in PBS and DW, as shown in **Fig. 10**. Within 24 h of submergence, the equilibrium swelling state was reached. The lyophilized hydrogels in an acidic environment showed the minimal swelling, but as the pH increases, the swelling percentage increased. The highest swelling rate of hydrogels was detected in distilled water. The swelling ratios of these hydrogels exhibited a constantly increasing trend in swelling as the degree of methacrylation decreased. **J. Nichol et al** [49] demonstrated that the degree of functionalization had a significant effect on the material's capacity, and tendency for absorbing and storing water molecules inside the polymer network. Conversely, maintaining the functionalization degree constant and decreasing the macromer concentration improved the mass swelling ratio.

The incorporation of small ratio of rGO has no influence on the swelling tendency of the hydrogel [27]. **K. R. Mamaghani et al** [40] found that the presence of these nano-scale materials with high concentrations occupied the hydrogel network space and reduced the penetration rate that restricted the swelling ratio of the hydrogel. Therefore, the variations in swelling percentage within Gel-MA(M1) and Gel-MA/rGO composite hydrogels were insignificant, since rGO did not covalently interact with the Gel-MA hydrogels. The ability of the prepared Gel-MA/rGO composite to absorb a huge quantity of water (almost 2444%) within 24 h of immersion provides a humid environment for the cells to proliferate in many medical applications.

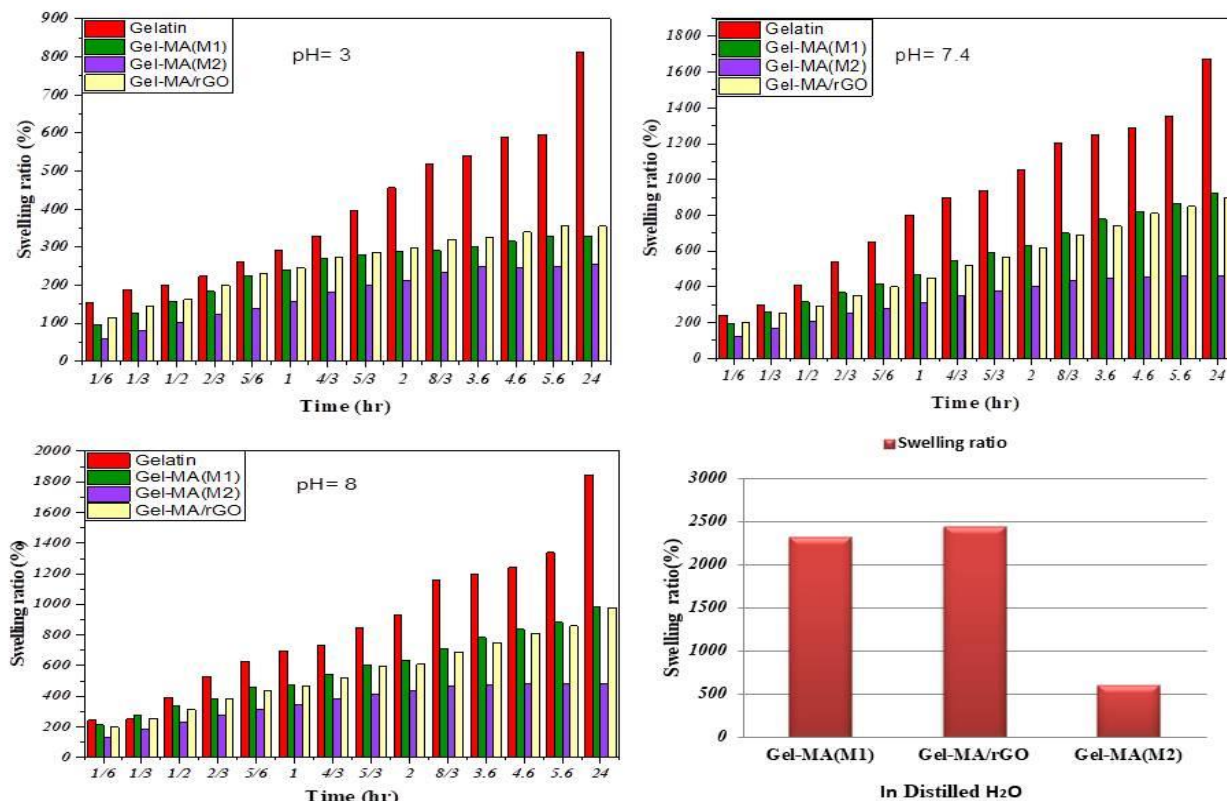


Fig. 10. Swelling ratio of gelatin, Gel-MA (M1), Gel-MA (M2) and Gel-MA/rGO hydrogels at different pH (3, 7.4 and 8) and in distilled water (DW).

3.2.10. Porosity of hydrogels

The porosity of the prepared lyophilized hydrogels is one of the important features to encourage fluid absorption and transport. The hydrogel porosity seems to be dependent on the crosslinking density as it decreased from low functionalization of Gel-MA(M1) to high one Gel-MA(M2) as displayed in **Fig. 11**. The porosity of (M1), (M2), and Gel-MA/rGO was found to be 68 %, 35% and 60 %, respectively. **S. Chakraborty et al** [50] and **Y. Kim et al** [51] confirmed that the addition of rGO to the hydrogel has almost no effect on the porosity of the hydrogel. As the incorporation of rGO nanoparticles did not significantly affect the freezing or sublimation rate of the aqueous solvent, resulting in similar porosity values for all the hydrogels. However, **T. Tang et al** found that an rGO-based aerogel displays a more pronounced porosity than an aerogel in the absence of rGO, they attributed this conclusion to the fact that the high porosity may rationalize the relatively high water swelling properties of rGO due to their hydrophilic groups [52]. Finally, our swelling results coincide with that of porosity ones which may support its dependence on the crosslinking density.

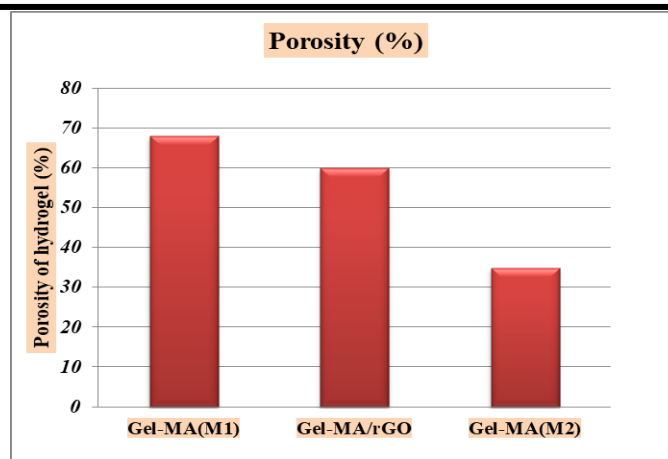


Fig. 11. Porosity of lyophilized hydrogels in n.Hexane.

3.2.11. Antimicrobial assay

Many reports have revealed that rGO can attack gram-positive and gram-negative bacteria. Nevertheless, size, type of bacteria, and shape significantly affect the level of the antimicrobial activity [53].

The benefits of Ag ions and Ag nanoparticles include their efficacy against both Gram-positive and Gram-negative bacteria, and a multifaceted mechanism of action. This mechanism translates into attacking the bacteria on several fronts (e.g. blocking respiration by binding to bacterial DNA, binding to enzyme to block energy cycle, binding to protein disulfide bridges to disrupt function), which makes it difficult for bacteria to develop resistance. This gives silver advantages compared to traditional antibiotics which typically target only a single site of the bacterium cell. Importantly, Ag nanoparticles show low or no cytotoxicity to human cells and reduce inflammation [29].

The present study explores whether it is possible to complement membranolytic and oxidative activity of rGO with the free radical formation of silver nanoparticles. **Fig. 12 a,b** shows the evaluation of the antibacterial activity of Gel-MA(M1), Gel-MA/rGO, and Gel-MA/rGO/Ag composite hydrogels against four pathogenic bacteria, two gram +ve (*S. aureus* and *B. subtilis*) and two gram -ve (*E. coli* and *P. vulgaris*) and the results are presented in **Fig. 13**. Recently, research has focused on the antibacterial efficiency of graphene and its hybrid materials. It was reported that rGO displayed a significant antibacterial activity. The antimicrobial action of rGO was associated to membrane stress caused by the sharp edges of graphene nano-sheets, which may cause physical damage to cell membranes, resulting in the loss of bacterial membrane stability and RNA leakage [54]. **X. Cai et al** prepared

nanocomposite hydrogel by anchoring the Ag-NPs on the rGO surface in order to increase the stability of Ag-NPs and enhance the role of rGO to kill bacteria [55].

By insertion of rGO, the inhibition of bacteria were enhanced to 80% for *E. coli*, 82% for *S. aureus*, 100% for *B. subtilis* and 26% for *P. vulgaris*. Furthermore, all hydrogels loaded with Ag-NPs (Gel-MA/rGO/Ag) exhibited much better antibacterial efficiency which could reach to 100%.

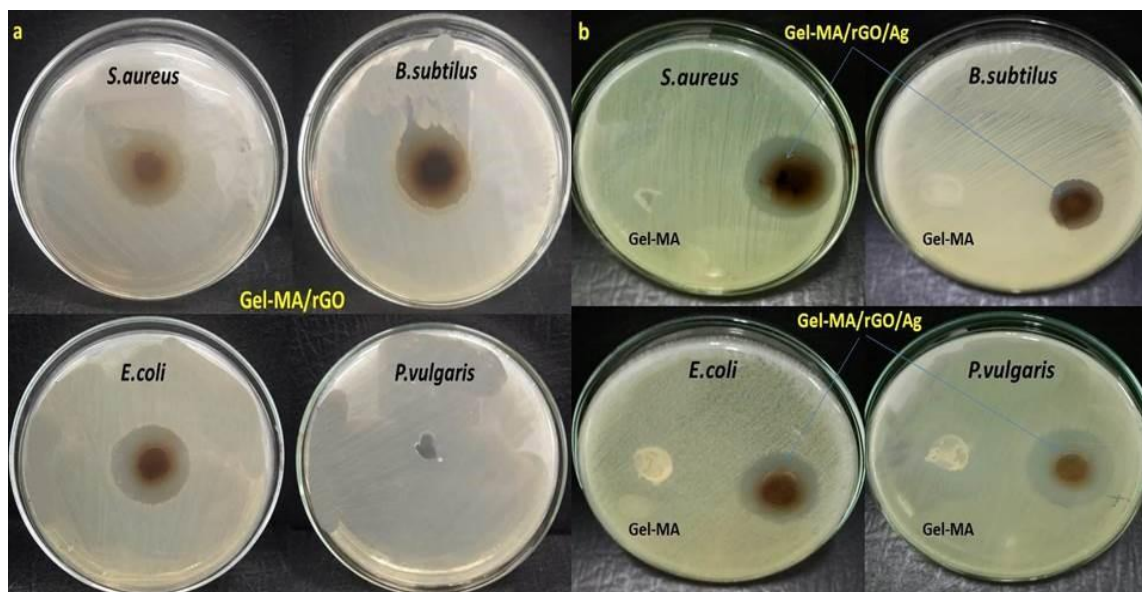


Fig. 12. Antimicrobial assay of a) Gel-MA/rGO, and b) Gel-MA and Gel-MA/rGO/Ag nanocomposite hydrogels.

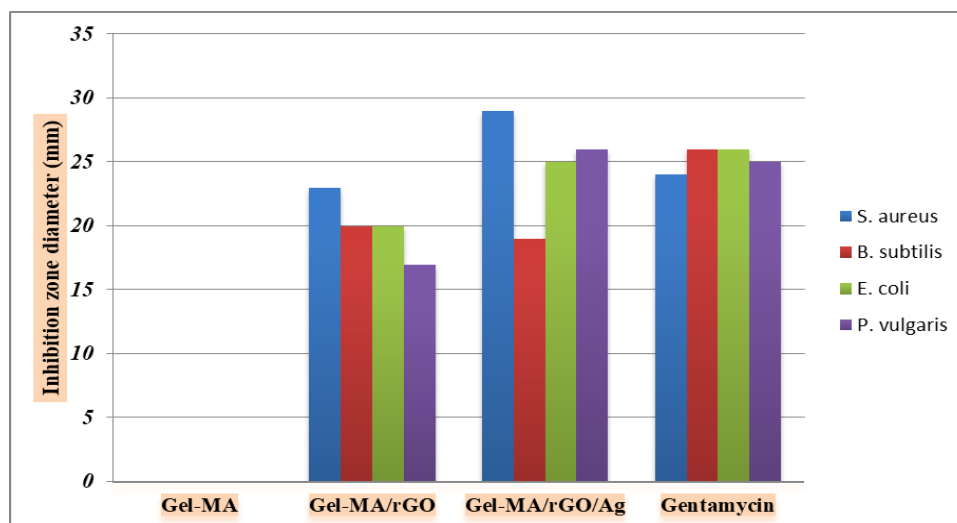


Fig. 13. Inhibition zone of Gram -ve and Gram +ve bacteria for Gel-MA, Gel-MA/rGO, Gel-MA/rGO/Ag nanocomposite hydrogels.

3.2.12. Antitumor activity: Cytotoxicity study

The prepared Gel-MA/rGO and Gel-MA/rGO/Ag composite hydrogels demonstrated a considerable cytotoxicity against human lung cancer (A549) cells and showed enhanced cytotoxicity in A549 cells at various doses. The MTT assay was used to quantitatively assess the toxicity of the samples since cell viability depends on the activity of cellular mitochondria. Gel-MA/rGO and Gel-MA/rGO/Ag composites were applied to cells for 24 h at increasing concentrations and the cell viability and morphological changes were analyzed. **Fig.14a** obviously demonstrates the percent of lung cancer cell inhibition with various concentrations of rGO composite. It was found that the IC_{50} (half-maximal inhibitory concentration) of Gel-MA/rGO is $109\mu\text{g/ml}$ against A549 cells, which reveals that Gel-MA/rGO composite showed enhanced anticancer capability. Furthermore, compared to Gel-MA/rGO composite, the Gel-MA/rGO/Ag composite exhibited a stronger inhibitory effect on the cell viability with IC_{50} of $27\mu\text{g/ml}$ against the A549 cells. The remarkably improved anticancer activity of Gel-MA/rGO/Ag is not basically due to the cumulative effects of the two components (rGO and Ag-NPs), but the cells may accumulate significantly much more Ag-NPs when they are attached to rGO sheets, which may be a result of the strong intracellular delivery capabilities of rGO sheets [56]. The IC_{50} values achieved from this manuscript are significantly lower than other previous studies. For instance, **T. Kavinkumar et al** [57] found $160\mu\text{g/ml}$ as IC_{50} value for rGO against A549 cells. According to this statement, testing Gel-MA/rGO exhibits effective activity against lung cancer cells even at very low concentrations. In addition to this, **D. Zhang et al** [58] found that the anticancer effectiveness of bio-synthesized Ag-NPs only against A549 cells was observed at a concentration of $40\mu\text{g/ml}$ by using cytotoxicity assay. Thus the current study demonstrated the strong efficacy of combining silver and rGO against lung cancer cells, which combines the properties of silver and rGO against human lung cancer.

The microscopic pictures of these two plates assayed by crystal violet staining are shown in **Fig. 14b**. Chemotherapeutics and other substances can be tested for their impact on a culture's growth and survival of cells using crystal violet assay. During cell death, adherent cells typically separate from culture plates, so this method can be used to quantify cell death after stimulation with death-inducing drugs and demonstrate variations in cell proliferation. By binding crystal violet to DNA and proteins in cells, it can dye the nucleus a deep purple and be used to check for permanent cell adherence. In Gel-MA/rGO and Gel-MA/rGO/Ag composites, the percent cell viability was greatest at the lowest concentration, and the percent cell inhibition increased as the concentration increased. As a result, the monolayer was destroyed, the number

of cells reduced, and the size of the remaining cells shrank remarkably. In the negative control, untreated cells with no morphological change were observed.

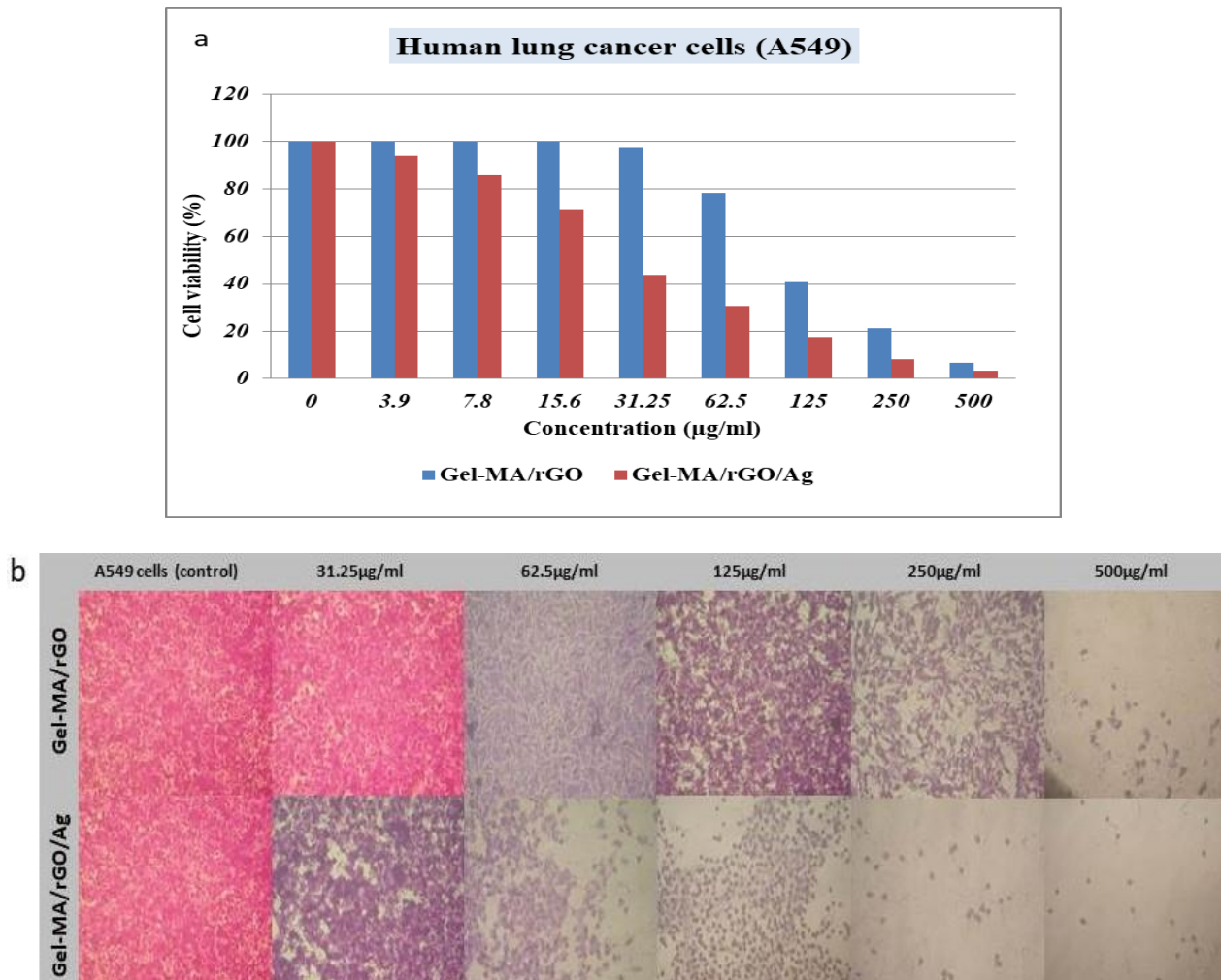


FIG. 14. (A) ANTICANCER PERFORMANCE OF NANOCOMPOSITES, (B) MICROSCOPIC IMAGES OF VARIOUS CONCENTRATIONS OF NANO COMPOSITES AGAINST LUNG CANCER (A549) CELL LINE.

4. Conclusion

This work was engaging with the synthesis and evaluation of Gel-MA/rGO and Gel-MA/rGO/Ag hydrogel composites against some model bacteria and human lung cancer cells in order to study the synergistic effect of both particles relative to their antimicrobial and anticancer efficacies. The antibacterial activity of Gel-MA/rGO and Gel-MA/rGO/Ag nanocomposites was evaluated against two gram +ve (*S. aureus*, *B. subtilis*), and two gram -ve (*E. coli*, and *P. vulgaris*) species and showed significant results against them compared to the virgin Gel-MA. All hydrogels loaded with Ag-NPs (Gel-MA/rGO/Ag) exhibited much better antibacterial efficiency which could reach to 100%. The Gel-MA/rGO/Ag composite displayed

significant cytotoxicity with an IC₅₀ of 27 μg/ml towards A549 cancer cells than that of Gel-MA/rGO (109 μg/ml). In the future study, these composites will be evaluated in vivo, taking into account their electrical stimulation responses due to the superior electrical conductivity of rGO.

Declaration of Competing Interest

Authors have declared no conflict of interest for publication of this work.

Acknowledgments

Authors gratefully acknowledge Ain Shams University for samples analysis for this research.

Reference

- [1] C. L. Ventola, The Antibiotics Resistance Crisis, *Compr. Biochem.* 11 (2015) 181–224.
- [2] G. Housman, S. Byler, S. Heerboth, K. Lapinska, M. Longacre, N. Snyder and S. Sarkar., Drug resistance in cancer: An overview, *Cancers (Basel)*. 6 (2014) 1769–1792.
- [3] J. Jeevanandam, A. Barhoum, Y. S. Chan, A. Dufresne, and M. K. Danquah, Review on nanoparticles and nanostructured materials: History, sources, toxicity and regulations, *Beilstein J. Nanotechnol.* 9 (2018) 1050–1074.
- [4] K. Kasinathan, K. Marimuthu, B. Murugesan, S. Samayanan, S. J. Panchu, H. C. Swart, S. R. I. Savariroyan., Synthesis of biocompatible chitosan functionalized Ag decorated biocomposite for effective antibacterial and anticancer activity, *Int. J. Biol. Macromol.*, 178 (2021) 270–282.
- [5] S. R. Mudshinge, A. B. Deore, S. Patil, and C. M. Bhalgat, Nanoparticles: Emerging carriers for drug delivery, *Saudi Pharm.* 19 (2011) 129–141.
- [6] D. Kichukova, I. Spassova, A. Kostadinova, A. Staneva, and D. Kovacheva, Facile Synthesized Cu–RGO and Ag–RGO Nanocomposites with Potential Biomedical Applications, *Nanomaterials*. 12 (2022) 12.
- [7] S. Kargozar, S. Ramakrishna, and M. Mozafari, Chemistry of biomaterials: future prospects, *Curr. Opin. Biomed. Eng.* 10 (2019) 181–190.
- [8] T. Biswal, S. K. BadJena, and D. Pradhan, Sustainable biomaterials and their applications: A short review, *Mater. Today Proc.* 30 (2020) 274–282.
- [9] N. El-tohamy, M. Attia, S. M. Easa, and N. M. Awad, Characterization and evaluation of nanocomposites chitosan-multiwalled carbon nanotubes as broad-spectrum antibacterial agent, *J. Sci. Res. Sci.* 35 (2018) 16–27.
- [10] T. H. Abdalla, N. Kandile, A. Nasr, D. Harding, and G. Bassioni, New modified chitosan composites and nanocomposites for different applications, *J. Sci. Res. Sci.* 38 (2021) 187–209.
- [11] M. Luo, K. Shaitan, X. Qu, A. P. Bonartsev, and B. Lei, Bioactive rare earth-based inorganic-organic hybrid biomaterials for wound healing and repair, *Appl. Mater.* 26 (2022) 101304.
- [12] E. Chiani, A. Beaucamp, Y. Hamzeh, M. Azadfallah, A. V. Thanusha, and M. N. Collins, Synthesis and characterization of gelatin/lignin hydrogels as quick release drug carriers for Ribavirin, *Int. J. Biol. Macromol.*, 224 (2023) 1196–1205..
- [13] G. P. Udayakumar, S. Muthusamy, B. Selvaganesh, N. Sivarajasekar, Biopolymers and

- composites: Properties, characterization and their applications in food, medical and pharmaceutical industries, *J. Environ. Chem. Eng.* 9 (2021) 105322.
- [14] Q. Dong, D. Wu, M. Li, and W. Dong, Polysaccharides, as biological macromolecule-based scaffolding biomaterials in cornea tissue engineering: A review, *Tissue Cell.* 76 (2022) 101782.
- [15] C. Polesca, H. Passos, J. A. P. Coutinho, and M. G. Freire, Sustainable Development Of Biomaterials Using Ionic Liquids, *Curr. Opin. Green Sustain. Chem.* 37 (2022) 100675.
- [16] Z. Li, Y. Li, C. Chen, and Y. Cheng, Magnetic-responsive hydrogels: From strategic design to biomedical applications, *J. Control. Release.* 335 (2021) 541–556.
- [17] S. Khaled, H. Zaky, A. Salah Nasr, and nadia hassan, Modified Chitosan Hydrogels and Nano Hydrogels for Congo Red Removal from Aqueous System, *J. Sci. Res. Sci.* 38 (2021) 91–117.
- [18] S. Mitura, A. Sionkowska, and A. Jaiswal, Biopolymers for hydrogels in cosmetics: review, *J. Mater. Sci. Mater. Med.* 31 (2020) 31–50.
- [19] C. Zhao, L. Zhou, M. Chiao, and W. Yang, Antibacterial hydrogel coating: Strategies in surface chemistry, *Adv. Colloid Interface Sci.* 285 (2020) 102280.
- [20] S. M. K. Uddin, M. A. M. Hossain, S. Sagadevan, M. Al Amin, and M. R. Johan, Halal and Kosher gelatin: Applications as well as detection approaches with challenges and prospects, *Food Biosci.* 44 (2021) 101422.
- [21] M. A. Sakr, K. Sakthivel, T. Hossain, S. R. Shin, S. Siddiqua, J. Kim, K. Kim, Recent trends in gelatin methacryloyl nanocomposite hydrogels for tissue engineering, *J. Biomed. Mater. Res.* 110 (2022) 708–724.
- [22] T. A. Arica, M. Guzelgulgen, A. A. Yildiz, and M. M. Demir, Electrospun GelMA fibers and p(HEMA) matrix composite for corneal tissue engineering, *Mater. Sci. Eng.* 120 (2020) 111720.
- [23] I. E. P. Souza, L. V. Cambraia, V. S. Gomide, and E. H. M. Nunes, Short review on the use of graphene as a biomaterial –prospects, and challenges in Brazil, *J. Mater. Res. Technol.* 19 (2022) 2410–2430.
- [24] K. K. H. De Silva, H. H. Huang, and M. Yoshimura, Progress of reduction of graphene oxide by ascorbic acid, *Appl. Surf. Sci.* 447 (2018) 338–346.
- [25] T. T. T. Phan, T. T. Truong, H. T. Huu, L. T. Nguyen, V. T. Nguyen, H. L. Nguyen, and V. Vo, Visible Light-Driven Mn-MoS₂/rGO Composite Photocatalysts for the Photocatalytic Degradation of Rhodamine B, *J. Chem.* 2020 (2020) 1-10.
- [26] S. William, JR. Hummers, R. E. Offeman., Preparation of graphitic oxide. *J. Am. Chem.* 80 (1958) 1339.
- [27] S. R. Ur Rehman, R. Augustine, A. A. Zahid, R. Ahmed, M. Tariq, and A. Hasan, Reduced graphene oxide incorporated gelma hydrogel promotes angiogenesis for wound healing applications, *Int. J. Nanomedicine.* 14 (2019) 9603–9617.
- [28] T. Sadeghi Rad, A. Khataee, F. Vafaei, and S. Rahim Pourn, Chromium and cerium co-doped magnetite/reduced graphene oxide nanocomposite as a potent antibacterial agent against *S. aureus*, *Chemosphere.* 274 (2021) 129988.
- [29] K. Prasad, G. S. Lekshmi, K. Ostrikov, V. Lussini, J. Blinco, M. Mohandas, K. Vasilev, S. Bottle, K. Bazaka & K. Ostrikov., Synergic bactericidal effects of reduced graphene

- oxide and silver nanoparticles against Gram-positive and Gram-negative bacteria, *Sci. 7* (2017) 1–11.
- [30] X. Yao, Z. Yan, X. Wang, H. Jiang, Y. Qian, and C. Fan, The influence of reduced graphene oxide on stem cells: A perspective in peripheral nerve regeneration, *Regen. Biomater.* 8 (2021) 1–9.
- [31] P. P. A. Jose, M. S. Kala, A. V. Joseph, N. Kalarikkal, and S. Thomas, Reduced graphene oxide/silver nanohybrid as a multifunctional material for antibacterial, anticancer, and SERS applications, *Appl. Phys. A Mater. Sci. Process.* 126 (2020) 1–16.
- [32] L. D. Geoffrion, T. Hesabizadeh, D. M. Cruz, M. Kusper, P. Taylor, A. V. Crua, J. Chen, A. Ajo, T. J. Webster, and G. Guisbiers, Naked Selenium Nanoparticles for Antibacterial and Anticancer Treatments, *ACS Omega*, 5 (2020) 2660–2669.
- [33] M. Sohail, M. Saleem, S. Ullah, N. Saeed, A. Afridi, M. Khan, M. Arif, Modified and improved Hummer's synthesis of graphene oxide for capacitors applications ☆, *Mod. Electron. Mater.* 3 (2017) 110–116.
- [34] B. Gürnlü, Ç. Taşdelen Yücedağ, and M. R. Bayramoğlu, Green Synthesis of Graphene from Graphite in Molten Salt Medium, *J. Nanomater.* 2020 (2020) 1-12.
- [35] J. M. Zatorski, A. N. Montalbino, J. E. Ortiz-Cárdenas, and R. R. Pompano, Quantification of fractional and absolute functionalization of gelatin hydrogels by optimized ninhydrin assay and ¹H NMR, *Anal. Bioanal. Chem.* 412 (2020) 6211–6220.
- [36] S. B. Balakrishnan, S. Kuppuppu, and S. Thambusamy, Biologically important alumina nanoparticles modified polyvinylpyrrolidone scaffolds in vitro characterizations and its in vivo wound healing efficacy, *J. Mol. Struct.* 1246 (2021) 131195.
- [37] M. F. Abo-Ashour, W. M. Eldehna, A. Nocentini, A. Bonardi, S. Bua, H. S. Ibrahim, 3-Hydrazinoisatin-based benzenesulfonamides as novel carbonic anhydrase inhibitors endowed with anticancer activity: Synthesis, in vitro biological evaluation and in silico insights, *Eur. J. Med. Chem.* 184 (2019) 111768.
- [38] S. Nedunchezian, C. W. Wu, S. C. Wu, C. H. Chen, J. K. Chang, and C. K. Wang, Characteristic and Chondrogenic Differentiation Analysis of Hybrid Hydrogels Comprised of Hyaluronic Acid Methacryloyl (HAMA), Gelatin Methacryloyl (GelMA), and the Acrylate-Functionalized Nano-Silica Crosslinker, *Polymers (Basel)*. 14 (2022) 2003.
- [39] C. Zhuang, F. Tao, and Y. Cui, Anti-degradation gelatin films crosslinked by active ester based on cellulose †, *RSC Advances*. 5 (2015) 52183–52193.
- [40] K. R. Mamaghani, S. Morteza Naghib, A. Zahedi, and M. Mozafari, Synthesis and microstructural characterization of GelMA/PEGDA hybrid hydrogel containing graphene oxide for biomedical purposes, *Mater. Today Proc.* 5 (2018) 15635–15644.
- [41] S. N. Alam, N. Sharma, L. Kumar, Synthesis and Characterization of Graphene Oxide (GO) and Reduced Graphene Oxide (rGO) for Gas Sensing Application, *Macromolecular Symposia*. 376 (2017) 1700006.
- [42] S. Darvishi, M. Souissi, M. Kharaziha, and F. Karimzadeh, Electrochimica Acta Gelatin methacryloyl hydrogel for glucose biosensing using Ni nanoparticles-reduced graphene oxide: An experimental and modeling study, *Electrochim.* 261 (2018) 275–283.
- [43] A. Hessein and A. A. El-Moneim, Developing cost effective graphene conductive coating and its application as counter electrode for cds quantum dot sensitized solar cell, *Proc. World Congr. New Technol.* 307 (2015) 1–9.

- [44] Y. Murali Mohan, K.Vimalaa, V. Thomasb, K.Varaprasada, B. Sreedharc, S .K .Bajpaib, K. M. Rajua, Controlling of silver nanoparticles structure by hydrogel networks, *J. Colloid Interface Sci.* 342 (2010) 73–82.
- [45] W. Xiaoa, J. Lib, X. Qub, L. Wanga, Y. Tana, K. Lia, H. Lib, X. Yueb, B. Lia, and X. Liao, Cell-laden interpenetrating network hydrogels formed from methacrylated gelatin and silk fibroin via a combination of sonication and photocrosslinking approaches, *Mater. Sci. Eng.* 99 (2019) 57–67.
- [46] S. Akmaz, E. Dilaver Adgüzel, M. Yasar, and O. Erguven, The effect of ag content of the chitosan-silver nanoparticle composite material on the structure and antibacterial activity, *Adv. Mater. Sci. Eng.*, 2013 (2013) 12–18.
- [47] S. Verma, V. K. Pandey, and B. Verma, Facile synthesis of graphene oxide-polyaniline-copper cobaltite (GO / PANI / CuCo₂ O₄) hybrid nanocomposite for supercapacitor applications, *Synth. Met.* 286 (2021) 117036.
- [48] M. Das, T. R. Aswathy, S. Pal, and K. Naskar, Effect of ionic liquid modified graphene oxide on mechanical and self-healing application of an ionic elastomer, *Eur. Polym. J.* 158 (2021) 110691.
- [49] J. W. Nichol, S. T. Koshy, H. Bae, C. M. Hwang, S. Yamanlar, and A. Khademhosseini, Cell-laden microengineered gelatin methacrylate hydrogels, *Biomaterials*,. 31 (2010) 5536–5544.
- [50] S. Chakraborty, T. Ponrasu, S. Chandel, M. Dixit, and V. Muthuvijayan, Reduced graphene oxide-loaded nanocomposite scaffolds for enhancing angiogenesis in tissue engineering applications, *R. Soc. Open Sci.* 5 (2018) 172017.
- [51] Y. Kim, W. S. Kim, and J. Lee, Graphene-reinforced collagen hydrogels with through-thickness porosity, *Macromol. Res.* 22 (2014) 813–815.
- [52] T. Tang, K. Goossens, S. J. Lu, D. Meng, and C. W. Bielawski, Agar-reduced graphene oxide selectively adsorbs organic dyes and strengthens double-network hydrogels, *RSC Adv.* 10 (2020) 29287–29295.
- [53] N. S. Ahmad, N. Abdullah, and F. M. Yasin, Toxicity assessment of reduced graphene oxide and titanium dioxide nanomaterials on gram-positive and gram-negative bacteria under normal laboratory lighting condition, *Toxicol. Reports*, 7 (2020) 693–699.
- [54] I. Sengupta, P. Bhattacharya, M. Talukdar, S. Neogi, S. K. Pal, and S. Chakraborty, Bactericidal effect of graphene oxide and reduced graphene oxide: Influence of shape of bacteria, *Colloids Interface Sci. Commun.*, 28 (2019) 60–68.
- [55] X. Cai, M. Lin , S. Tan, W. Mai, Y. Zhang, Z. Liang, Z. Lin, X. Zhang, The use of polyethyleneimine-modified reduced graphene oxide as a substrate for silver nanoparticles to produce a material with lower cytotoxicity and long-term antibacterial activity, *Carbon N. Y.*, 50 (2012) 3407–3415.
- [56] K. Modaresifar, A. Hadjizadeh, and H. Niknejad, Design and fabrication of GelMA/chitosan nanoparticles composite hydrogel for angiogenic growth factor delivery, *Artif. Cells, Nanomedicine Biotechnol.* 46 (2018) 1799–1808.
- [57] T. Kavinkumar, K. Varunkumar, V. Ravikumar, and S. Manivannan, Anticancer activity of graphene oxide-reduced graphene oxide-silver nanoparticle composites, *J. Colloid Interface Sci.*, 505 (2017) 1125–1133.
- [58] D. Zhang, G. Ramachandran, R. A. Mothana , N. A. Siddiqui, R. Ullah, O. M. Almarfadi,

G. Rajivgandhi, Natesan Manoharan., “Biosynthesized silver nanoparticles using *Caulerpa taxifolia* against A549 lung cancer cell line through cytotoxicity effect/morphological damage, *Saudi J. Biol. Sci.*, 27 (2020) 3421–3427.

المُلخَص العَرَبِي

مركبات الفضة الهيدروجيلية النانوية القائمة على الجرافين لمضادات الجراثيم والأورام: التقييم في المختبر

أسماء خالد عاطف أ - تحية بيومي مصطفى أ - حازم محمد الشريف ب

أ. قسم الكيمياء - كلية البنات لأداب و العلوم و التربية - جامعة عين شمس - مصر الجديدة - القاهرة - جمهورية مصر العربية

ب. قسم البوليمرات و المخضبات - المركز القومي للبحوث - القاهرة - جمهورية مصر العربية

إن كفاءة معظم علاجات السرطان والمضادات الحيوية محدودة بسبب العديد من المشكلات ، بما في ذلك مقاومة الأدوية والآثار السلبية غير المحددة. تم استخدام الهيدروجيل القائم على مشتق الجرافين و الجسيمات النانوية الفضية (Ag-NPs) للتغلب على هذه القيود. في هذا العمل، تم تحضير الهياكل الهجينة (Gel-MA) و تفاعله مع المواد النانوية النشطة الوظيفية ، تم تصنيع أكسيد الجرافين المخفض (rGO) باستخدام حمض الأسكوربيك كعامل مختزل لتكوين مركب مع Gel-MA دون التأثير على الخصائص الفريدة لـ Gel-MA. وتم توصيف rGO و الهلاميات الهيدروجيلية المركبة التي تم إعدادها باستخدام التقنيات الطيفية المعتادة. ولقد تم استخدام مقايسة Ninhydrin لقياس درجة الأداء الوظيفي. و بقياس درجة الانتفاش مع الماء وجدنا ان مركب النانو تضخم بنسبة 2444 % بسبب المسامية العالية للهيدروجيل. و اوضحت النتائج أن هيدروجيل النانو المركب أظهر نشاط مضاد للميكروبات أعلى من المركب (Gel-MA). ثم تم فحص السمية الخلوية لمركبات Gel-MA / rGO و Gel-MA / rGO / Ag ضد سرطان الرئة في الانسان A549 باستخدام فحص MTT. أظهر ان مركب Gel-MA / rGO / Ag له سمية خلوية كبيرة بقيمة IC_{50} تبلغ 27 ميكروغرام / مل تجاه خلايا A549 مقارنة بتلك الموجودة في Gel-MA / rGO 109 ميكروغرام / مل.